

Numerical and experimental Investigations of Slot Flow with Respect to Wind Tunnel Wall Interference Assessment

S.A. Glazkov, A.R. Gorbushin, A.I. Ivanov, A.V. Semenov, V.V. Vlasenko *
(Central Aerohydrodynamic Institute, Russia)

J. Quest °
(European Transonic Windtunnel, Germany)

This paper presents the results of an experimental investigation of the flow field near the slotted wall of a transonic wind tunnel. Distributions of three components of the disturbed velocity are obtained as well as the limiting streamlines patterns on the wall. The parameters of the linearized boundary condition on the slotted wall modeling the European Transonic Wind Tunnel (ETW) wall geometry are defined. Preliminary results of a numerical simulation of the viscous turbulent flow around a single slot are also presented. The calculations demonstrate coherent, large-scale, quasi-periodic non-stationary motions of low energy gas within the slot duct.

Nomenclature

a	= slot width;
a_0, A_0	= free term in slotted boundary conditions;
B	= test section width; coefficient in slotted boundary conditions;
C_p	= pressure coefficient;
d	= slot spacing;
ETW	= European Transonic Wind Tunnel;
h	= distance from the wall;
K	= coefficient of the streamlines curvature in slotted wall boundary condition;
M	= Mach number;
n	= normal to the surface;
U_∞	= free stream velocity;
$PETW$	= ETW pilot facility;
R	= porous-wall parameter;
R^2	= correlation coefficient;
Re	= Reynolds number;
$ISTC$	= International Science and Technology Center;
t	= slot depth;
U_x, U_y, U_z	= disturbed velocity components;
x, y, z	= Cartesian system of coordinates;
$X_{probe} Y_{probe} Z_{probe}$	= X- Y- Z- coordinates of the probe nose;
α	= model angle of attack, upwash;
β	= sidewash;
δ	= boundary layer thickness;
σ	= RMS value;
χ	= sweep angle;
θ	= streamline angle;
v	= normal velocity component;
δ^*	= boundary layer displacement thickness;
φ	= potential of the disturbed velocity.

* Senior Researcher
° Chief Aerodynamicist, Senior AIAA Member

Copyright © by European Transonic Windtunnel & Central Aerohydrodynamic Institute, Russia.
Published by the American Institute of Aeronautics and Astronautics, Inc. with permission.

I. Introduction

In recent years, the manufacturers of transport aircrafts have been imposing more and more stringent requirements for the accuracy of experimental investigations in wind tunnels. This is caused by the needs for a more reliable determination of the aerodynamic characteristics of the aircraft and, accordingly, its economic effectiveness. Striving for most accurate performance measurements in wind tunnels requires an enhanced knowledge of interference effects introduced by the flow boundaries. Considering slotted wall wind tunnels, the subject appears extremely complex due to the presence of a strong 3-dimensional slot flow and the non-homogenous boundary conditions.

One of the main aspects of increasing the accuracy of experimental investigations in wind tunnels is improving the accuracy of methods accounting for the flow boundary effect on the aerodynamic characteristics of a model under study. It is known that almost for any method used to determine the flow boundary effect it is necessary to have mathematically formulated boundary conditions on the test section walls. The accuracy of determining the boundary conditions will govern the error of calculated corrections for the flow boundary effect. This problem is also the case for the European Transonic Wind tunnel (ETW) with the test section having slotted walls.

Several groups of investigators (Davis and Moore¹; Chen and Mears²; Baldwin, Turner and Knechtel³; Goethert⁴; Wood⁵; Baronti, Ferri and Weeks⁶; Berndt and Sorensen⁷; Barnwell⁸; Everhart and Barnwell⁹; Everhart, Igoe and Flechner¹⁰; Freestone and Mohan¹¹ and others) were engaged in investigations in order to obtain a simplified flow model near the slotted wall and to formulate the boundary condition. They considered diverse wall configurations: different numbers of slots and their configurations, different slot open area ratios, wall width and slot cross section geometry etc. In spite of the growing potential of computer engineering and equipping of wind tunnels with up-to-date measuring facilities, at the present time the "correction" methods based on the classical theory remain to be prevailing in the world practice. Their improvement is basically aimed at refining the boundary conditions for real wind tunnels and extending to previously uncovered fields of investigation (high angle of attack, transonic conditions etc.).

The statement of the slotted-wall interference problem and the methods of its solution for potential flows are well surveyed in the classical publication¹² devoted to flow boundary interference in subsonic wind tunnels and numerous papers concerning walls with longitudinal slots^{1,3,13-18}.

The ideal uniform boundary condition on the slot boundary derived from the balance of differential pressure on the wall and flow curvature near the slot^{1,3,4} is as follows:

$$\varphi_x + K\varphi_{xn} + \frac{\varphi_n}{R} = 0$$

where R is the parameter governing viscous differential pressure on the wall, K is the parameter related to geometric dimensions of slots.

Generally, modernization of the classical boundary condition does not concern the form of the boundary condition. It is basically focused on refinement of the coefficients and their dependence on different parameters (wall thickness, boundary layer state, external disturbance intensity, etc.).

The classical value of K is generally found assuming that the flow is two-dimensional, inviscid and for slots of infinite length. In the Ref. 1 the wall thickness is taken as zero, while the theory² refined in Ref. 8 accounts for the wall thickness. As a result, the coefficient K in these cases differs almost two times. The experimental data on determining K are rather dissimilar because they are obtained in diverse wind tunnels, on walls with different geometric dimensions of slots and under different conditions (Mach numbers, model types etc.). It is obvious that such incomplete database prevents a reliable determination of the coefficient K in every particular case.

A rather effective inviscid theory of slotted wall interference was developed by Berndt⁸. Later, Sedin and Sorensen¹⁹ revealed viscosity effects to be of considerable importance and should be taken into account in constructing the theory of slot boundaries even in the case when this theory is mainly based on equations for inviscid fluid. Nevertheless, scarcity of experimental information was noted which prevented obtaining a more correct flow field model.

To improve the understanding of the physics of slot flows and to elaborate suitable boundary conditions for CFD application for an assessment of wall interference in the European Transonic Wind Tunnel (ETW), a cryogenic pressurized facility, the flow situation was modeled in one of the small TsAGI wind tunnels (T-125). Experiments were carried out both in the empty wind tunnel and in the presence of suitable models (symmetrical 10% airfoil with 50mm chord and a half-model with semi-wing span of 150mm and a MAC of 37mm). The main operating condition corresponded to the flow Mach number of ~ 0.8 and the unit Reynolds number of $\sim 19.5 \cdot 10^6 \text{ m}^{-1}$.

In parallel with experiments, a numerical simulation of the flow in the slotted wall test section of ETW was performed. Calculations were based on full 3D compressible non-stationary Favre-averaged Navier-Stokes equations, closed by a (q- ω)-model of turbulence. The mathematical model includes the complete detailed geometry

of a single slot as well as parts of the ETW test section and of the plenum chamber. Presently, only a preliminary stage of these calculations is finished. The goals of this stage: to acquire an experience of simulating viscous turbulent flow in such a complex geometry, to develop the methodology of calculation, to test the numerical method and code. So, at this stage calculations were performed without reproducing all conditions of ETW flow. Nevertheless, some qualitative comparison with experimental was made. In addition, some interesting physical effects of the slot flow were revealed.

II. The Technique of simulating the ETW test section flow in the TsAGI T-125 wind tunnel and experimental equipment

The experimental investigation carried out in the TsAGI T-125 wind tunnel for the purpose of simulating the flow in the European transonic cryogenic wind tunnel, ETW, was scheduled as the basis of the experimental part of the work. Prior to the start of the work at the stage of selecting an appropriate test facility, a general concept of the experimental approach to the problem was established and basic simulation criteria were formulated. It was evident from the very beginning that it was impossible to simulate perfectly the ETW flow conditions because of the very high Reynolds numbers achieved at cryogenic conditions, therefore, this area was not covered. The simulation parameters used in the experiment were basically resulting from the experience of the previous work²⁰ and the analysis of the literature devoted to slot boundaries.

The experiment was planned so that the two interconnected tasks stated below could be solved:

1. To obtain data on the flow structure near the slotted walls, in the plenum chamber and inside the slot channels with the aim of verification of the numerical methods used to calculate such flows.
2. To measure distributions of pressure, velocity components, as well as partial derivatives of these parameters in order to formulate a homogenous distributed boundary condition for the slotted walls of ETW.

In compliance with this statement, the ETW wall simulation concept was developed for the T-125 wind tunnel, as well as the experimental program and the relevant equipment.

The European cryogenic wind tunnel, ETW, is designed for testing complete vehicle models and half-models at sub- and transonic flow velocities under ordinary ambient conditions as well as applying the cryogenic technologies. In the latter case, the temperature of the working gas (nitrogen) is down to $\sim 110^{\circ}\text{K}$ and the flow Reynolds numbers reach flight numbers.

The wind tunnel has a $2.4\text{m}\times 2.0\text{m}$ test section with a length of $\sim 9\text{m}$ (Fig. 1).

The vertical walls are parallel, while the horizontal walls can have different inclination angles to optimize the axial pressure gradient in the test section. Two boundary versions can be realized in the wind tunnel, solid smooth walls and slotted boundaries. The horizontal walls are provided with 6 slots of complex geometry. At the end of the test section, in the re-entry zone, the panels between the slots (slats) become tapered, thus forming wedge-like structures. The geometry of the slot cross-section is rather complex. It is worth to note such structural features as contoured divergent channels at the interface of the test section and the diffuser, as well as a great depth of the slots. At the end of the test section, a regulated gas auto-suction from the plenum chamber is organized using special finger flaps. The standard wall angle with open slots is equal to 0.55° divergence, while the finger flap setting angle is 7° outward. Velocity profiles in the boundary layer measured on the walls demonstrate not only an increase in the thickness of the boundary layer (and its integral characteristics) as the flow moves downstream, but also a change in the profile shape, a decrease in the flow momentum, approaching the separation state of the boundary layer.

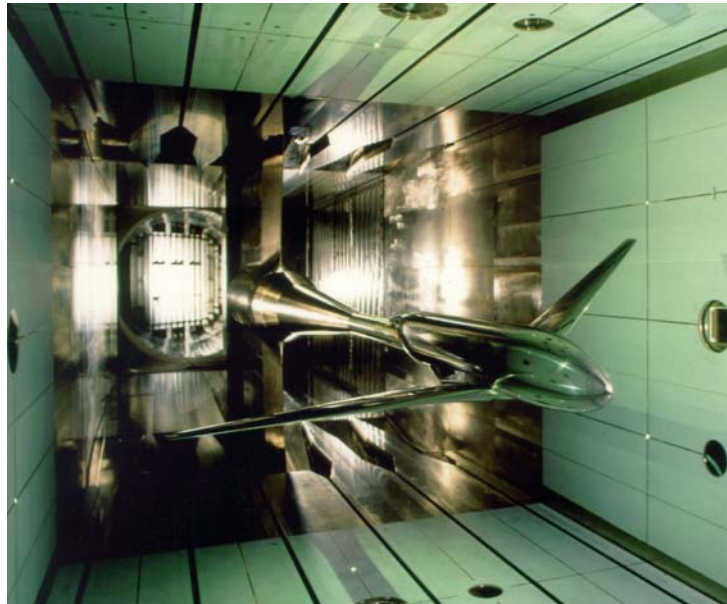


Figure 1: ETW with model used for numerical simulations.

The TsAGI T-125 wind tunnel is a blow-down continuous-operating facility designed as a low-turbulence wind tunnel. It is characterized by a flow contraction ratio of more than 20 and is equipped with damping screens and noise suppressors. The first test section is intended for smooth nozzle inserts to achieve subsonic conditions and supersonic conditions up to $M = 4.0$ with intervals of 0.5. The second test section is provided with perforated and slotted subsonic inserts. The total pressure in the plenum chamber can be varied over a wide range (from 2×10^4 Pa to 4×10^5 Pa) at almost constant stagnation temperature (in the order of 273°K). The T-125 wind tunnel is equipped with optical windows to observe the model and to take images and videos.

Test section №1 was taken as a baseline one because of great optical windows on the side walls enabling the flow to be watched not only inside the test section but also outside of it. The previous experience²⁰ revealed that it was of particular importance to attain similarity in criterion d/δ^* , where δ^* is the boundary layer displacement thickness and d is the linear dimension characteristic of the permeable wall (in this case, it is the slot width or the distance between the slots). This criterion is satisfied approximately for the 1:6 model. This scale allows the complete model of the slot wall to be arranged in the plenum chamber by maintaining a required relationship between the slot width and depth.

The modified test section of T-125 is shown in Fig. 2. Keeping the smooth subsonic ceiling unchanged, it became possible to manufacture a new lower insert simulating one-half of the ETW floor. In this case, the height of the test section was about 180mm with a length of about 1500mm and a width of 200mm. In view of the fact that only a quarter of the ETW section could be simulated, the resulting asymmetry about the axis was of no importance. In the zone of the first optical window two model types could be installed: 1) two-dimensional wing airfoils; 2) half-models. These models were mounted on the hand-driven α -mechanism. The geometry of three slots corresponds to the ETW slot configuration. The diameter of the optical windows is greater than the test section height, which is convenient for flow visualization within the slots as the permeable wall section nearest to the windows is partially made of a transparent material (organic glass). The remaining parts are made of aluminum alloy, which facilitated both manufacturing and modernization of the elements. Particular emphasis in designing was placed on the rear part of the slot panel. The reentry zone with finger flaps was reproduced exactly in geometry by providing both the correct wall and finger flap angle.

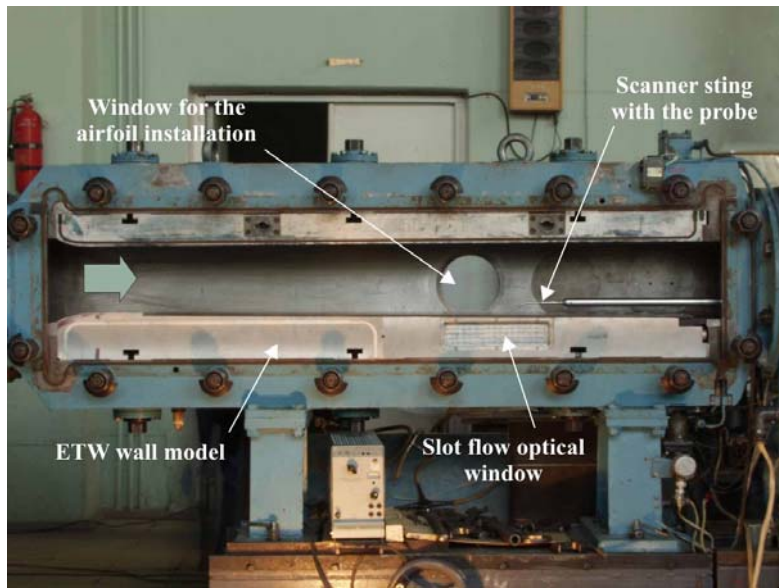


Figure 2: T-125 experimental set-up.

The limited shell volume of the T-125 prevents a correct simulation of the ETW plenum chamber; however, the ETW plenum chamber is three-dimensional and envelopes the total test section. The global simulation of the ETW flow proves to be unfeasible, therefore attention was focused on local phenomena.

The test program included a cycle of investigating flow fields both with the model and without it. In both cases, detailed measurements of pressure distributions along one of the floor slats, as well as in the transverse slot sections were suggested. These measurements were supplemented by wall boundary layer investigations.

The test program included a cycle of investigating flow fields both with the model and without it. In both cases, detailed measurements of pressure distributions along one of the floor slats, as well as in the transverse slot sections were suggested. These measurements were supplemented by wall boundary layer investigations.

As a recording system, electronic scanners with multi-channel pressure modules were used. Pressure values measured by the probe were recorded by differential Kistler transducers. The most important part of the program was the scanning of the flow field near the slots by using microprobes. After manufacturing and calibration, a 5-hole probe was capable of measuring the velocity magnitude and direction at a specified point with a great accuracy introducing minor disturbances into the flow. The second type of the microprobe enabled measurements of static pressure distributions in the flow with a good resolution.

The X-Y-Z traversing mechanism located in the wind tunnel diffuser allows (when using booms of different lengths) an essential survey of the flow field of the whole region under investigation. The accuracy of installing the probe using the X-Y-Z mechanism in all three axes is only limited by the discreteness of rotation counters; the minimum interval is 0.15mm.

The most interesting flow zones were visualized using color oils or tufts. The visualization results were recorded on photos- and video films with subsequent decoding and interpretation.

The calibration of the 5-hole microprobe intended for measuring the total pressure, as well as upwash and sidewash, was accomplished according to the standard technology in the range of $\pm 8^\circ$ for both pitch and sideslip angles.

The probes shaft shows a curved design (to allow for measurements in the boundary layer and inside the slot) and a hemispherical head of 1mm dia. with discrete bores of ~ 0.15 mm.

The following should be noted: The classical approach for obtaining the pressure-flow angle dependencies works well in flows without pronounced viscous effects, of which most significant is the velocity profile (and total pressure) shift. If this fact is not taken into account, when measuring, e.g. the upwash in the boundary layer above the lower wall, an error in the form of an "imaginary upwash" will be introduced comparable to a measured quantity. Although, despite of its miniature dimensions, the probe does not allow for measurements of all pressures at the identical position (the distance between the axes of opposite holes is 0.6mm to 0.7mm). It is easy to see that in this case the "imaginary upwash" will be of negative sign ("towards the wall"). To take into account this phenomenon, the "imaginary upwash" was measured in a classical boundary layer near the standard tunnel ceiling with an inclination angle to horizon of 0.1° with the predictable flow inclination. Correction to α reach about 2° when calculated for the streamline angle. A similar correction to β was not applied to the results.

III. Investigation of flow fields near the ETW slotted wall model in the TsAGI T-125 wind tunnel

The next stage after calibrations and installation of the basic equipment involved adjustment of the wind tunnel operating regimes. This process took much time because a new scheme of the test section produced off-design flow. After the analysis and selection of the facility parameters in the main series, the test group choose the stable condition at $M \approx 0.8$ and $P_t \approx 1.2 \cdot 10^5$ Pa for reference.

The main part of the experiment implied measurements of the flow parameters and pressure distributions near the slotted boundary simulating $\frac{1}{4}$ of the ETW slotted wall. The measurements were made in the empty wind tunnel, as well as using two types of models attached to the α -mechanism on the side wall. The first model was a symmetrical airfoil with a thickness ratio of 10% and chord of 50mm installed at angles of attack of $\pm 4.5^\circ$, $+8.5^\circ$ and -0.5° . Then, a half-model was tested. It featured a swept half-wing (sweep angle at the leading edge $\chi = 33^\circ$) and a supercritical airfoil with a thickness of 10%, $MAC = 37$ mm and a span of 150mm, the trailing edge being characterized by a sweep break.

The half-fuselage features 15mm in diameter and 240mm in length (Fig. 3).

The axis of rotation in α for both models corresponded to the coordinate $X = 813$ mm and passed through the section of 40 % of the airfoil chord or at a distance of 137mm from the half-model nose. A schematic view of the wind tunnel and its respective coordinate system are shown in Fig. 4.



Figure 3: Half-model in T-125 wind tunnel.

From here on, the measuring sections $Z=0$ (axis of the central slot and the whole lower wall), $Z = \pm 4.5$ mm, ± 9 mm, ± 27 mm and ± 36 mm (axis of slats) were used.

Scanning the flow field, the free-stream parameters were measured at each test point, as well as the pressure distributions along one of the lower wall slats, in one of its cross sections and in three sections inside the slot according to the scheme given in Fig. 4. The selected approach allowed estimating the interference effect of the X, Y, Z-scanner sting on the flow parameters.

A. The Flow field in the empty test section

The velocity profiles of the boundary layer were measured using the central orifice of the five-hole probe when scanning the flow field along the slotted wall and during the calibration measurements on the smooth upper wall. The

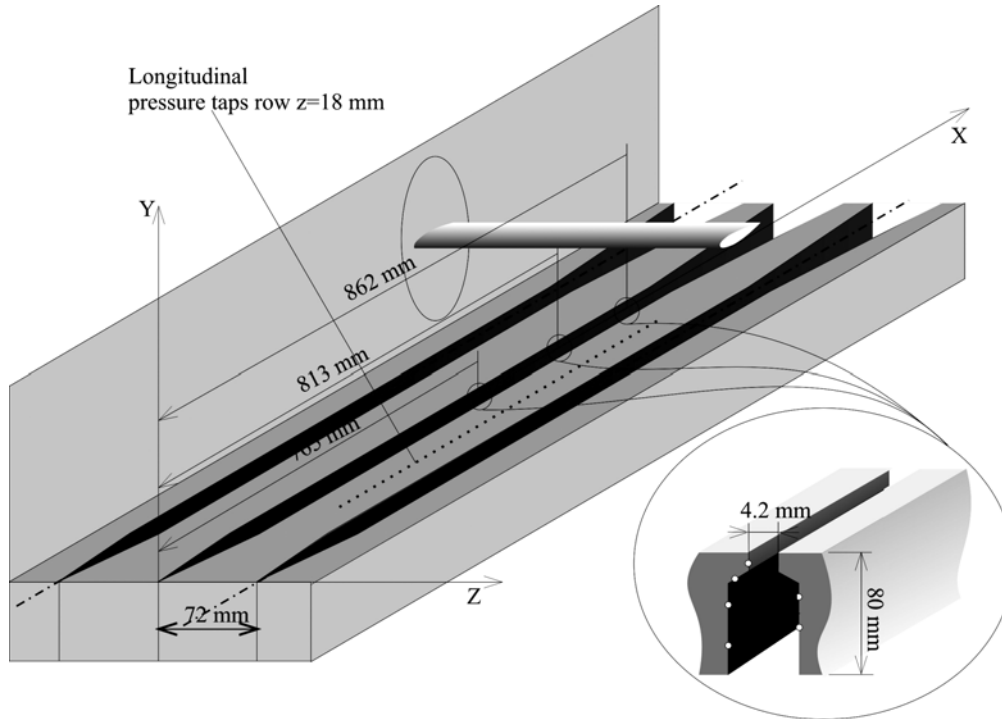


Figure 4: Geometrical scheme of the T-125 experiment.

comparison of velocity profiles obtained in the T-125 wind tunnel with the available data from ETW is of major importance, as it allows an assessment of the quality of flow simulation achieved in the T-125. For a comparison of the reduced velocity profiles, the transverse coordinates of points gained in the T-125 wind tunnel have been scaled by the ratio of longitudinal coordinates of respective sections; thus, all the data are conditionally reduced to the corresponding ETW coordinates.

Comparing the results obtained on the T-125 smooth wall with relevant ETW data demonstrates a good agreement and a classical "turbulent" shape of the velocity profiles. On the slotted wall, comparisons are presented for several axial positions where ETW data have been available (Fig. 5). Good agreement on the velocity profiles in the central region of the tunnel as well as further downstream document a comparable flow development in both facilities. In particular, a decreased flow momentum status in the boundary layer and an approach of the velocity profiles to the pre-separated status are to be noted which indicates the same flow history. Such similarity of the profiles spreads a certain optimism with respects to an adequate simulation of other parameters of the ETW flow and, accordingly, the boundary conditions on the slotted wall.

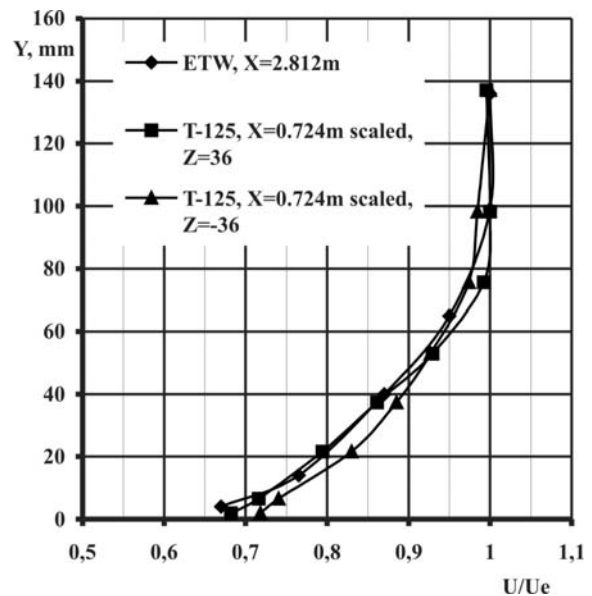


Figure 5: Comparison of ETW and T-125 B.L. profiles on slotted walls.

The axial distributions along the surface were investigated at several distances from the wall. The measurements were limited along the axis X from 724mm to 979mm (i.e., from -89mm to $+166\text{mm}$ with respect to the α -mechanism axis of rotation). The transverse sections corresponding to the longitudinal coordinates $X = 724\text{mm}$,

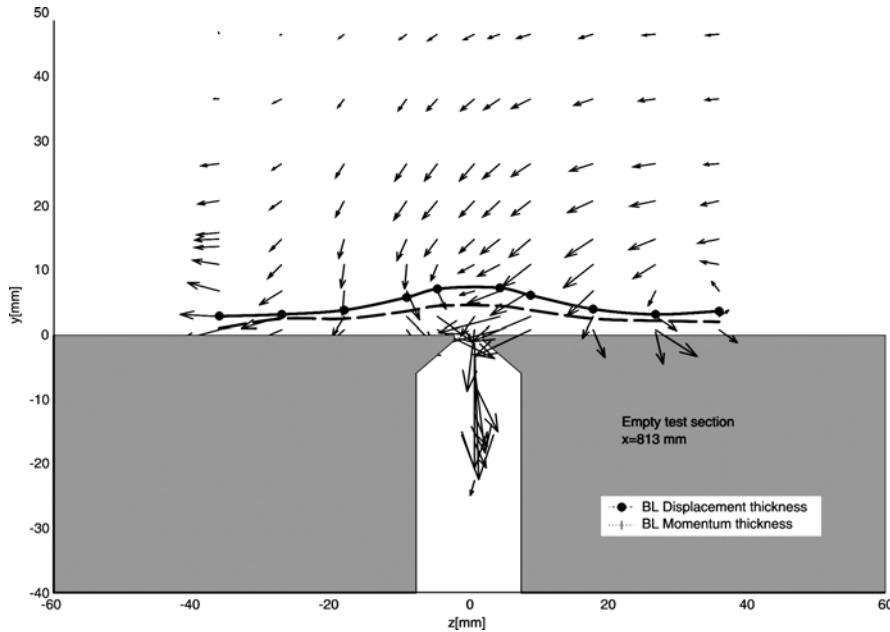


Figure 6: Distribution of V and W components of velocity.

- almost at $Z = |d/4|$ a line of 3D attachment must form;
- 3) In the range $d/4 < |Z| < d/2$ a vortex line with an axis directed downstream can be noticed. The vertical and transversal scales are almost the same to be $\sim d/4$. The direction of rotation is clockwise to the right

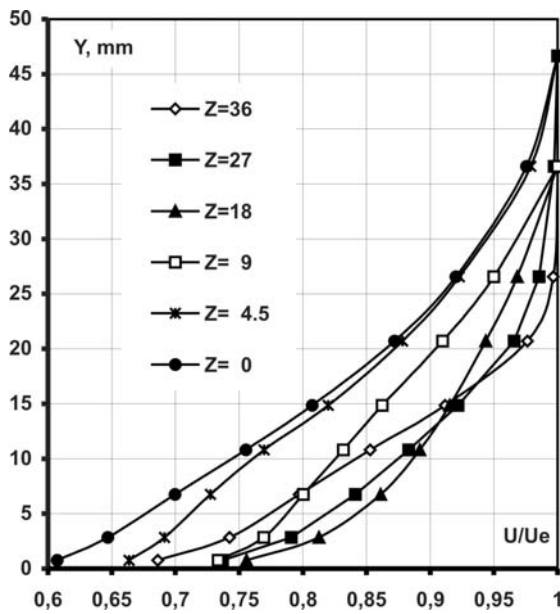


Figure 7: Boundary layer profiles, empty test section, $X = 813\text{mm}$.

813mm (α -mechanism axis) and 979mm were investigated as detailed as possible. The measured vertical and transversal velocity components at $X = 813\text{mm}$ are shown in Fig. 6. By analyzing the obtained results it is possible to outline several distinctive features of the flow:

- 1) Over the whole region under study, gas outflow prevails through the slots from the test-section into the plenum chamber;
- 2) Near the surface in zone $Z < |d/4|$, where $d=72\text{mm}$ is the reference inter-slot spacing, the flow is directed towards the slot, while in zone $d/4 < |Z| < d/2$ we are faced with the opposite situation; thus,

(downstream) of the slot and counterclockwise to the left.

Typical velocity profiles in the boundary layer are shown in Fig. 7 supplementing the flow pattern. It is clearly seen that the largest flow velocity near the wall ($Y < 15\text{mm}$) is noted in section $Z = 18\text{mm}$ ($d/4$) because the low-speed gas from the boundary layer is swept away from there by the transverse flow to adjacent sections. At the same time, at $Y > 15\text{mm}$, the flow pattern changes: now a higher-momentum flow is transferred from section $Z = 18\text{mm}$ ($d/4$) to section $Z = 36\text{mm}$ ($d/2$). Of particular interest is the flow directed upwards in the wall layer along the axis of the slat at $Z=36\text{mm}$. As a whole, it can be stated that the scale of the disturbed region at the wall appreciably exceeds the characteristic dimensions of the boundary layer on the smooth and even rough plate at the given Reynolds numbers. Its size is of the order of $d/2$ which is likely to be almost independent on the flow Reynolds number.

The profiles above the solid surface at $|Z|=d/2$ show an appreciable momentum loss similar to that fixed in the ETW test section.

B. Flow field in test section with models

In the tests using the 2-D model, the vertical sections were investigated within the range of Y from 0.5mm (above the solid boundary) and -20 mm (in the slot) to $Y = 50$ mm for the previously considered positions in X and Z .

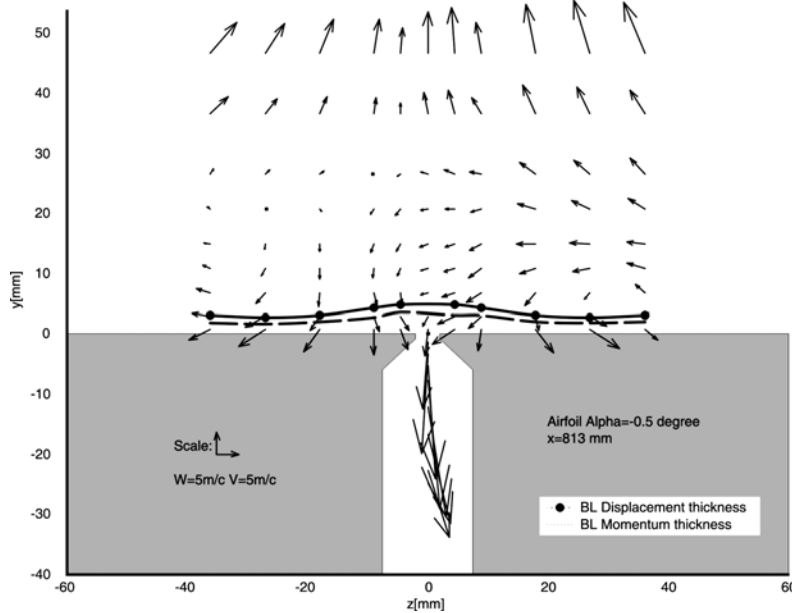


Figure 8: Distribution of V and W components of velocity.

flow field in the section corresponding to the model axis of rotation is given in Fig. 8 for an angle of attack of 0.5° . The presence of the model in the wind tunnel makes the flow more ordered and slightly decreases the size of the non-uniform flow region near the wall. For high angles of attack, the vortex structures on the sides of the slot are less pronounced although they are still noticeable. The flow at small model angles of attack is of complex nature and similar to the flow in the empty wind tunnel. It's interesting to note that, in spite of the upwash in the outer region, inflow into the slot prevails. A comparison of the upwash and sidewash in different transverse sections shows that for a relatively thick

shear layer (of the order of 35 to 40mm) all the parameters become equalized almost at the same distance from the wall; the boundary of the flow equalization region is approximately at a height of $d/2$ (36mm). This finding forms the basis for a consideration of a homogeneously distributed boundary condition for inviscid flow core.

The last stage of work involved investigations of the flow field near the ETW slotted wall model with the installed half-model. From the view of flow simulation in ETW such a configuration is the closest to the optimum one as, in a certain sense, it is equivalent to the scheme "full model + full wind tunnel". A significant difference from the original is the model position close to the lower wall and, as a consequence, a high level of disturbances. In the given test series, static pressure distributions were measured not only on the wall but also in the flow at three distances from the wall using a special probe. Summarizing, it may be stated that the flow direction at the wall is governed by the rotation direction of the vortex shedding from the wing tip. For example, the flow under the wing is directed to the right at $\alpha = +4^\circ$ and to the left at $\alpha = -4^\circ$.

C. Flow visualization near the slotted wall

Flow visualization on the slotted test section wall and inside the longitudinal slot was supposed to be performed by two methods: an oil film method and a tuft method. Because of the risk of getting paint into pressure taps, at the first stage only the second method was used. The flow was visualized using 12mm-long cotton threads bonded to the surface. The physical flow pattern was recorded through the side optical window of the test section by two video cameras with continuous recording in real time of the wind tunnel run and one digital photo camera. The test results are presented for $M = 0.8$ in the form of a series of four frames taken during one count of the pneumomeasurements, the time interval between frames being ~ 0.3 s. The photos demonstrate a significantly non-stationary and vortex flow with great upwash in the wide portion of the slot both in the empty wind tunnel and in the presence of the airfoil model. These results are in good agreement with pneumomeasurements of the velocity profile and upwash $\alpha(y)$. To illustrate the flow non-stationarity in the slot, the images obtained within interval of 1s are shown together in Fig. 9.

At the final stage of the experiment, the oil film method was used for flow visualization. This stage was of fundamental importance from the standpoint of understanding of the physical flow pattern near the slotted wall model. The recent experimental investigations (see, e.g., Ref. [22] in the wind tunnel with low level of initial flow turbulence $\varepsilon \sim 0.1\%$ using a three-component laser Doppler velocimeter) reveal that by an artificial boundary layer suction through a single micro-orifice on a flat plate, a pair of longitudinal vortex structures will be generated. It is

concluded from the flow visualization and pneumomeasurements using a microprobe that an analogy exists to the formation of the same type of longitudinal vortex structures in the turbulent boundary layer which was also observed in the present investigations of flow near the slotted wall of the test section both in the test section and in the plenum chamber.

Flow visualization was performed using an oil film with white and red pigments. The physical flow pattern was also recorded by video cameras and a digital photo camera. During the tests, images were taken through the side optical test section windows, while after the run the photo camera was used for the open side wall.

The oil film was covered in the form of transverse strips of oil with white pigment on the wall and with red pigment inside the slot. For the main test condition ($M = 0.8$), the flow pattern peculiarities are as follows (see Figs. 10, 11):

1. On the test section panel from the beginning of the slots and along them, an inflow into the slot has been recorded. In this case, a three-dimensional vortex structure is formed. This flow pattern is in agreement with the results of pneumomeasurements using a microprobe. The projection of the external vortex boundary is seen in the form of a displacement of streamlines from the slot boundaries.
2. The size of the displacement region along the test section length is not increased. At the end of the test section panel, in the "reentry" region, the limiting streamlines on the slot walls reveal an outflow from the cavity with formation of longitudinal vortex structures.
3. In the slot cavity (visualization of spreading the oil points with black pigments) the flow pattern is also complex: averaged streamlines demonstrate the formation of a system of alternating macrovortex structures.
4. The presence of the red oil paint track (oil paint is covered on the internal slot surfaces) on the external wall surface in zone of intense gas outflow from the test section demonstrates the phenomenon already observed by Berndt¹⁸: even with intense outflow, the stagnant gas at the slot edge can be ejected inside the turbulent flow.

The general flow pattern on the test section panel at different half-model angles of attack ($+4^\circ$ and -4°) is almost the same as in the empty wind tunnel except for a change in the zone of vortex sheet displacement in the region of half-model swept wing position. These data are also in good agreement with the results of the pneumomeasurements.

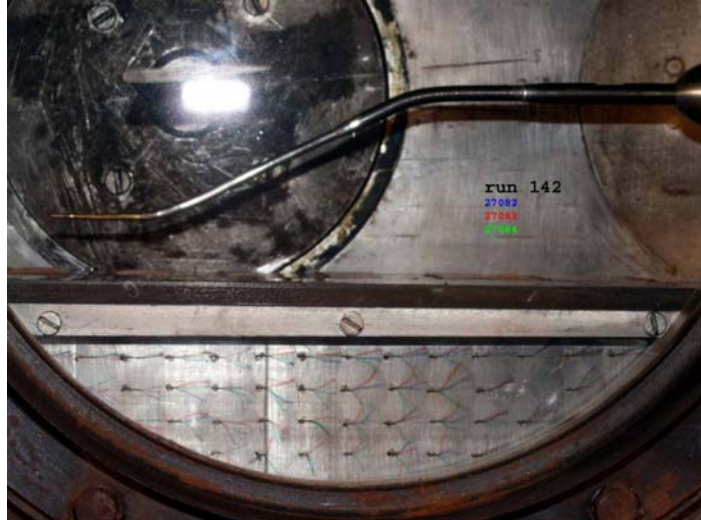


Figure 9: Graphical superposition of four successive frames obtained within time interval 1 second, $M=0.8$, $\alpha=-4.5^\circ$.



Figure 10: Empty test section. Oil visualization. Slot flow pattern (after run).

The flow visualization in the cavity under the slot (oil, tufts) also shows a complicated non-stationary pattern of vortex flow.

Fig. 11 shows the flow pattern obtained for the empty test section.

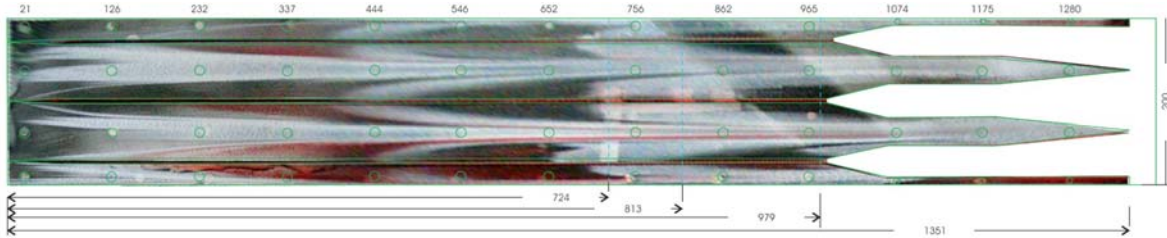


Figure 11: Empty test section. Oil visualization. Slot flow pattern (after run).

IV. Experimental determination of linear boundary condition in the PETW wind tunnel

An additional test series was carried out in the pilot wind tunnel PETW to investigate boundary conditions on the slotted walls. This facility is an exact copy of the ETW wind tunnel scaled 1:8.9 (Fig. 12) where the used five-hole probe is shown in front of a dummy sting-boss.

Especially for these tests a simplified model (cone-cylinder body and triangle wing) and a rake for the flow-inclination measurements were designed and fabricated. The arrangement of the pressure-probe rake and the model in the PETW test section is given in Fig. 13.

The upwash and total pressure near the wall were measured by a strut mounted series of five three-hole probes installed at different vertical positions. Changes in the model angle of attack at the rake location on the wall result in changes of the flow parameters – static pressure and upwash. The objective of the present study was to establish a simple functional relationship between the velocity components near the wall.



Figure 12: PETW wind tunnel.

The tests were carried out at atmospheric pressure and non-cryogenic flow regimes at Mach number ranging from 0.3 to 0.9.

The results of the upwash measurements were obtained with the probes for three settings of the horizontal walls over the whole velocity range. The data obtained with the model in place were tared to the empty tunnel measurements of corresponding configuration, which allowed to cancel out the individual rake effect on the flow field. According to the estimates made for a distance of $h \geq 0.5d = 22.5\text{mm}$ from the wall, which corresponds approximately to the position of probe 4, the flow is considered to be equalized in the transverse direction. Pressure distribution on PETW test section walls was also measured for each flow regime.

The form of the homogeneous boundary condition for wind tunnel slotted walls is considered above. For the particular case, the linearized boundary condition can be written as follows:

$$Cp_{wall} = \pm 2dK \frac{d\alpha}{dx} + A_0 \quad (2)$$

where sign "+" refers to the upper wall, while "-" concerns the lower wall, d is the distance between the slots. The Cartesian coordinate system is chosen and the flow direction coincides with axis X , while the upwash has positive sign ($\alpha > 0$), when directed along axis Y . In terms of the perturbation velocity components we have

$$\alpha \approx U_y / U_\infty = v, \quad \frac{d\alpha}{dx} \approx \frac{dv}{dx}, \quad \text{and} \quad Cp = -\frac{2U_x}{U_\infty} = -2u.$$

Eq. (2) can be integrated to obtain the relationship between the local upwash and the pressure integral:

$$\int_{x_0}^x Cp_{wall}(t)dt = \pm 2dK\alpha(x) + C_0, \text{ where } C_0 = A_0(x - x_0) \mp 2dK\alpha(x_0) \quad (3)$$

Assuming that the boundary conditions in the empty test section and with the model are the same, it is convenient to analyze Eqs. (3) in the form:

$$INT_Cp = \int_{x_0}^x (Cp_{wall}^{mod}(t) - Cp_{wall}^{empty}(t))dt = \pm 2dK \cdot ALPHA + C'_0, \text{ } ALPHA = \alpha^{mod}(x) - \alpha^{empty}(x)$$

The upwash value ALPHA is determined for probe 4.

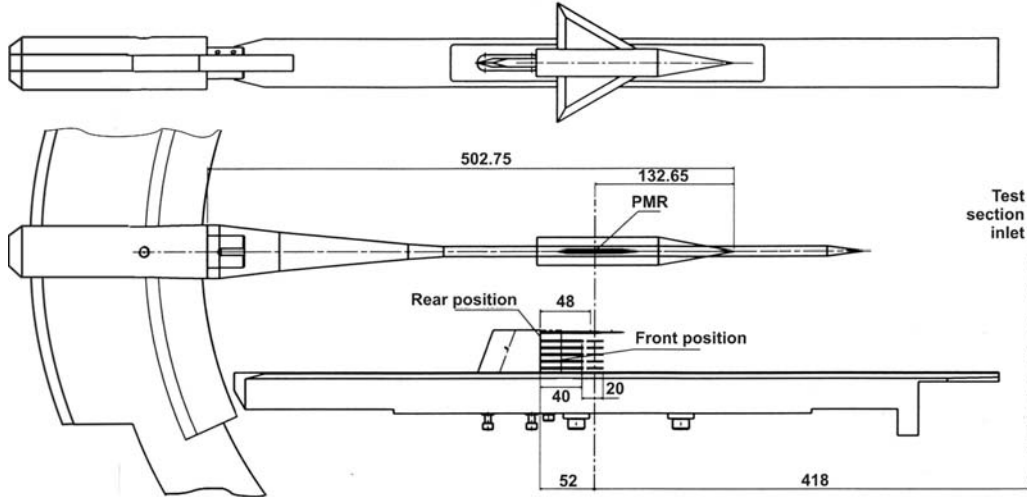


Figure 13: Geometrical scheme of PETW experiment.

Fig. 14 presents one of the obtained functional dependencies $INT_Cp(ALPHA)$ for the standard position of the horizontal walls. The linear approximation of the experimental data by the least square method demonstrates a high correlation approaching unity. The above approximation makes it possible to derive coefficients K for the boundary condition (Fig. 15) depending on the free-stream Mach number at different angles of the horizontal walls. Significant effect of the free-stream velocity on coefficient K is not to be seen.

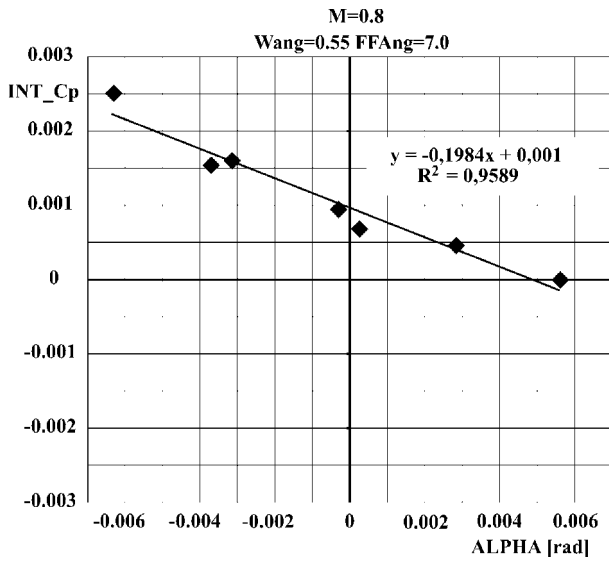


Figure 14: Cp integral/flow angle correlation.

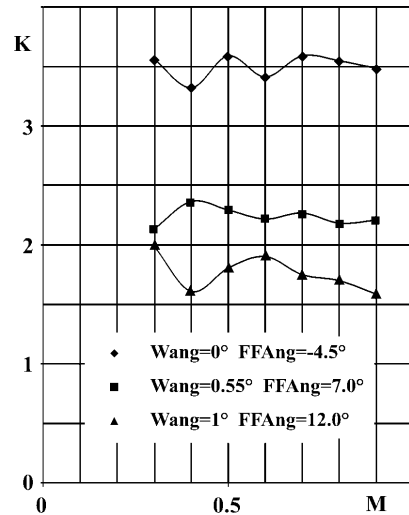


Figure 15: Coefficient K for the boundary condition, PETW.

V. Navier-Stokes calculations of a single slot flow

Numerical simulations of 3d viscous turbulent flow inside the ETW test section including slots and with plenum chamber would require too much computer memory and time for computation. But, computation costs may be reduced by a factor up to 10, if we only consider a simplified task of simulating a single slot.

To obtain a mathematical model of a single slot, we may consider to cut out a single slot channel assuming a lateral symmetry of the flow as given in the right of Fig 16. Thus, this mathematical model includes the detailed geometry of a single slot, including the re-entry region (with the re-entry flap, inclined by the angle of 7 deg), as well

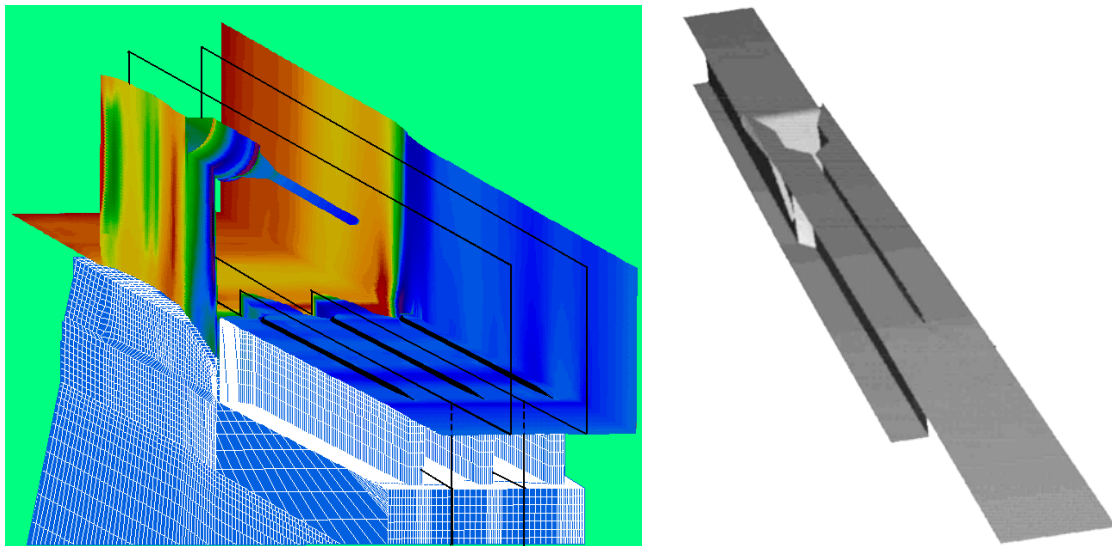


Figure 16: Mathematical model of single slot

as the correct depth and cross-section contour of the slot duct, with an additional bottom panel simulating the floor. This mathematical model also correctly represents the height of the ETW test section with the bottom wall, inclined by angle 0.55° , and a part of the plenum chamber.

The numerical method is characterized by a 2nd order approximation in space and time including an explicit Godunov-type TVD scheme for convective terms, an explicit central-difference approximation of the diffusive terms, and a point-implicit approximation of source terms in the equations for describing the turbulence parameters. To solve the problem of small time steps, a local time stepping was used. Details of the applied numerical method may be found in Ref. 21.

All computations were performed on a dual-processor personal computer (Pentium III 2×1000 Mhz).

The computational domain was built up by a regular multiblock grid. Special grid compressions were applied: 1) in the vicinity of mixing layers (in the slot and in the re-entry region; more than 50 cells were placed across this zone); 2) and especially – in the vicinity of no-slip solid walls (20 cells were placed across boundary layers with compression 1:100).

Compressed parts of the grid are rounded by blocks with relatively coarse, nearly uniform grid (20 cells across inviscid core of flow in ETW test section; 130 cells along the whole computational domain, in longitudinal direction). On the joint boundaries between blocks with fine and coarse grid, a boundary condition for irregularly connected grids is used. (This boundary condition allows grid lines to be discontinuous on boundaries between adjacent blocks.)

The total number of cells was 980000 resulting in a RAM requirement of about 2000MB.

The following flow condition was simulated: A Mach number of $M = 0.78$, a total pressure of $P_t = 197kPa$, and a total temperature of $T_t = 300^\circ K$. The turbulence parameters at the inlet of the computational domain were taken as $q = 2.7m/sec$ and $\omega = 200Hz$. On the bottom wall of the ETW test section and on the surface of the slot duct, the no-slip boundary condition was imposed. Other solid boundaries, as well as lateral vertical planes (which bound the computational domain) were treated as slip solid walls.

It has to be underlined that these Navier-Stokes calculations only reflect a preliminary solution as these calculations were aimed to acquire an experience of simulating viscous turbulent flow around such a complex

geometry and to develop a methodology for such calculations, as well as to test the numerical method and the code. So, at this early stage it was not considered to extensively simulate a series of different flow conditions. Consequently, attention should be given to the following details: Firstly, the real boundary layer at the test-section inlet of ETW was not properly simulated. Additionally, the computational domain in our calculations contains a constant-area buffer subregion upstream of the test section. The boundary layer grows from the beginning of this buffer subregion (from $x = -5$ m). As a result, the thickness of the boundary layer differs from reality at the entrance of the test section. Consequently, any comparison with boundary layer data measured in ETW may differ.

Also, no special inlet and exit boundary conditions were used in these calculations to establish a specific flow regime. Instead, Riemann boundary conditions were used both at the inlet and exit of the computational domain. The parameters for a determination of the Riemann invariants corresponded to a regime $M = 0.78$ but at the entrance of the computational domain the flow was established to $M = 0.753$.

Now let's consider some results of our calculations.

The most interesting result is the unsteady character of the numerical solution. The flow around a single slot doesn't converge to a steady state; instead, some unsteady processes proceed continuously. In Fig. 17, one may see fields of longitudinal velocity $u [m \cdot sec^{-1}]$ at sequential time slots (during one cycle of flow development). On the first picture, some elements of the geometry are shown. It may be noticed that the turbulent mixing layer is developing on the slot surface (on the bottom wall). In the re-entry region the flow interacts with the re-entry flap and is separated into two individual streams. One stream is directed to the right. The second stream is directed to the left, inside the slot duct. It propagates upstream to the middle part of the slot generating disturbances (upward displacement) of the mixing layer. This displacement results in a weakening of the flow interaction with the re-entry flap and therefore in a reduction of the second stream, which is generated on the re-entry flap. The latter effect results in the reverse downward displacement of the mixing layer. After that, this process repeats periodically.

But what is the character of this unsteady flow development? Is it periodic or not? To answer this question, we have analyzed time dependencies of the static pressure at several points on the lateral boundary of the computational domain. These dependencies are shown in Fig. 18; one may see that they have quasi-periodical character.

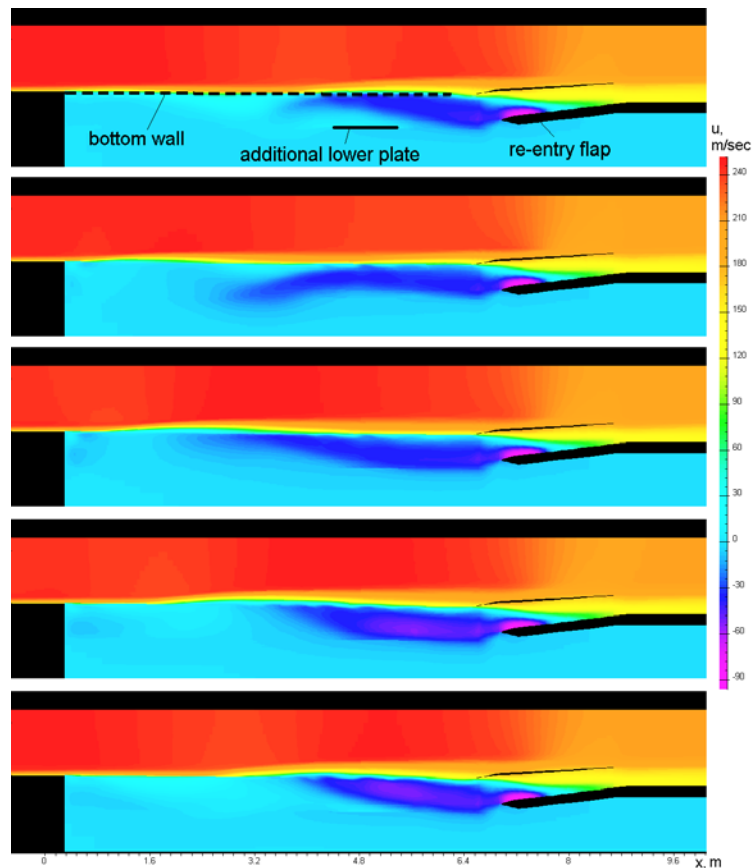


Figure 17: Flow development in the symmetry plane of slot.

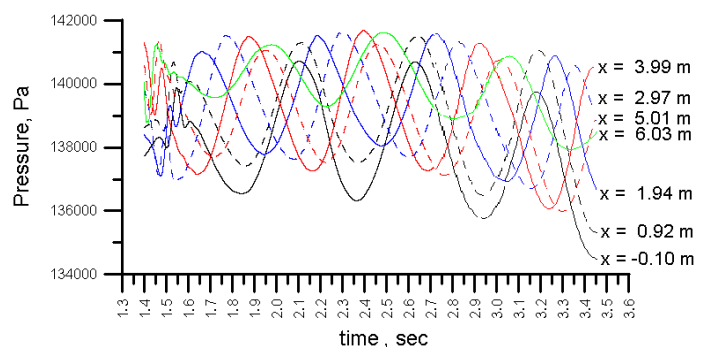


Figure 18: Time dependencies of pressure at several points on the lateral boundaries of the computational domain.

Therefore, the flow structure is changed periodically (despite of the fact that the computation has been performed on the basis of solving the time-averaged Navier-Stokes equations, closed by a $(q-\omega)$ model of turbulence). This result means that large-scale turbulence (including coherent structures), which cannot be simulated by classical semi-empirical models of turbulence, play a significant role in the slot flow. So, the use of a quasi-LES (Large Eddy Simulation) approach with a direct simulation of large-scale turbulence and with an approximated model for subgrid turbulence would be justified and reasonable. Such calculations will be the subject of future investigations.

The periodical character of the flow development gave us the idea to average the numerical solution in time. In the averaged field, all perturbations of the flow parameters disappeared. The Mach number above the slot became practically constant, also the total pressure along the test section.

Finally, we have compared results of the Navier-Stokes computations with experiments from the T-125 wind tunnel. Fig. 19 presents the computed field of longitudinal velocity for comparison with the experimental flow field given in Fig. 7. The distributions of the boundary layer displacement thickness and the momentum thickness, which are shown in the experimental picture, are similar (in shape) to the isolines of the longitudinal velocity gained by the computations. There also exist some differences between experiment and computation. The experimental picture reveals rather noticeable flow in the transverse direction; in the computational results (with symmetric geometry and with symmetric boundary conditions on the lateral boundaries) such transverse flow is not visible. To take this effect into account, it is planned to impose a special boundary condition on the lateral boundaries (using information from the T-125 experiments). Such computations – with a detailed reproduction of the T-125 conditions – will be made in the next future.

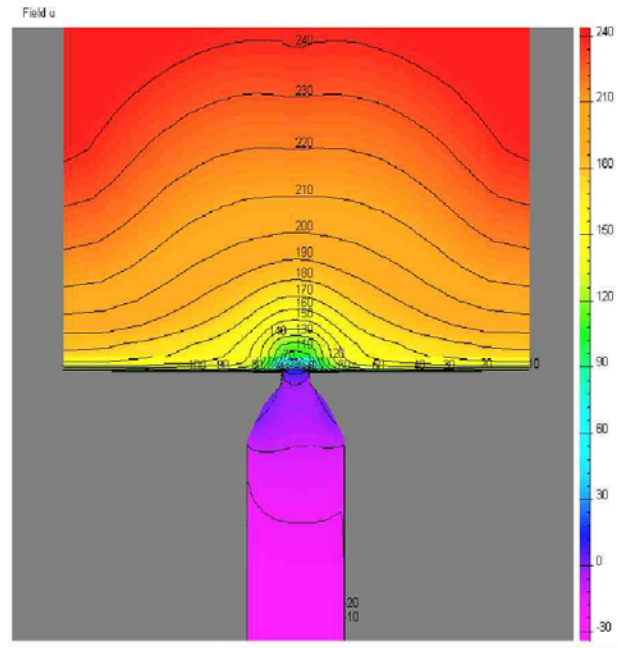


Figure 19: Single slot computation (field of longitudinal velocity, m/sec) for comparison with experimental data (Fig. 7).

VI. Conclusion

Results of a test campaign simulating the flow in the slotted wall European Transonic Wind Tunnel (ETW) by adaptation of the TsAGI T-125 wind tunnel are presented. The tests covered design and manufacturing of an ETW slotted wall model, the adjustment of experimental equipment and operational conditions, as well as the calibration of a universal probe in flow and measurements of flow fields near the slotted wall. The experiments were carried out both in the empty wind tunnel and in the presence of models (symmetrical 10% airfoil with chord of 50mm and half-model with semi-wing span of 150mm and $MAC = 37mm$). The main operating condition corresponded to the flow Mach number of ~ 0.8 and the unit Reynolds number of $\sim 19.5 \cdot 10^6 m^{-1}$.

The quantitative characteristics of the flow field (pressure distributions on the walls and within the slot, distributions of three velocity components and the static pressure in the zone above the slotted wall and inside of one of the slots) both in the empty wind tunnel and for different flow conditions with models have been obtained. The flow pattern was investigated and flow peculiarities for different model positions were identified above the slotted test section boundary. The flow similarity near the walls of the ETW and its corresponding model in the T-125 wind tunnel is documented. The behavior of the time-averaged characteristics allows the assumption that the statement of the distributed homogeneous boundary condition on the control surface beyond the viscous layer might be quite realistic. The scale factor of the equalization region is estimated $d/2$ for all the parameters, where d is the reference dimension (lateral slot spacing).

The investigations are supplemented by flow visualization near the surfaces using tufts distributed over the whole region under study (including the internal slot surfaces). The obtained photo- and video material demonstrates a significant unsteady flow behavior with an intense upwash especially pronounced in the region inside the slot. Flow visualization by the oil film method confirms the main results of pneumomeasurements.

A limited test cycle for flow near the pilot wind tunnel (PETW) wall was conducted. The determined uniform boundary conditions relying on the results obtained in the PETW wind tunnel and formulated on the reference surface, provide a sufficiently reliable simulation of the relationship of parameters beyond the viscous layer and are in good agreement with data from other sources.

The performed numerical simulation of the slot flow on the basis of solving the Navier-Stokes equations has revealed coherent, large-scale, quasi-periodic non-stationary flow movements in the slot duct. Analogous processes were observed in the experiment.

Acknowledgements

This work was accomplished in the framework of the ISTC Project #1978. The authors would like to thank the ISTC and its project manager G. Kulikov for their support, the project manager S. Bosniakov and the scientific manager V. Neyland for fruitful advices and discussions. The authors express their gratefulness to N. Mikhailov, A. Makashin, N. Khoziaenko and other TsAGI specialists for the help in T-125 experiment and to the staff of ETW for organizing and performing the PETW tests. Last but not least thanks are given to S. Mikhailov and to S. Matyash, who took part in numerical simulation of the single slot flow.

References

- ¹Davis D.D.Jr., Moore D. "Analytical study of blockage- and lift-interference corrections for slotted tunnels obtained by the substitution of an equivalent homogeneous boundary for the discrete slots", NACA RM L53E07b, June 1953.
- ²Chen C.F., Mears J.W. "Experimental and theoretical study of mean boundary conditions at perforated and longitudinally slotted wind tunnel walls", AEDC TR-57-20, 1957.
- ³Baldwin Jr.B.S., Turner J.G., Knechtel E.D. "Wall interference in wind tunnels with slotted and with slotted and porous boundaries at subsonic speeds", NASA TN 3176, 1954.
- ⁴Goethert B.H. "Transonic wind tunnel testing", Pergamon Press, New York, 1961.
- ⁵Wood W.W. "Tunnel interference from slotted walls", Quarterly J. of Mech. and Applied math., Vol. 17, May 1964, pp. 126-140.
- ⁶Baronti P., Ferri A., Weeks T. "Analysis of wall modifications in a transonic wind tunnel", ATL TR-181, 1973.
- ⁷Berndt S.B., Sorensen H. "Flow properties of slotted walls for transonic test sections", AGARD CP No. 174, Paper 17, 1975.
- ⁸Barnwell R.W. "Improvements in the slotted-wall boundary condition", Proceedings - AIAA 9th Aerodynamic Testing Conference, pp. 21-30, 1976.
- ⁹Everhart J.L., Barnwell R.W. "A parametric experimental study of the interference effects and the boundary-condition coefficient slotted wind tunnel walls", AIAA Paper 78-805, 1978.
- ¹⁰Everhart J.L., Igoe W.B., Flechner S.G. Slotted-wall flow-field measurements in a transonic wind tunnel", NASA TM-4280, 1991.
- ¹¹Freestone M.M., Mohan S.R. "Interference determination for wind tunnels with slotted walls", AGARD CP-535, "Wall interference and flow field measurements", Paper 19-1, 1993.
- ¹²Garner H.C., Rogers E.W.E., Acum W.E.A., Maskell E.C. "Subsonic wind tunnel corrections", AGARDograph 109, 1966.
- ¹³Acum W.E.A. "Note on the evaluation of solid-blockage corrections for rectangular wind tunnels with slotted walls", A.R.C. R&M 3297, 1961.
- ¹⁴Holder D.R. "Upwash interference in a rectangular wind tunnel with closed side walls and porous slotted floor and roof", A.R.C. R&M No. 3322, 1962.
- ¹⁵Holder D.R. "Upwash interference on wings of finite span in a rectangular wind tunnel with closed side walls and porous-slotted floor and roof", A.R.C. R&M No. 3395, 1965.
- ¹⁶Pindzola M., Lo C.F. "Boundary interference at subsonic speeds in wind tunnels with ventilated walls", AEDC TR-69-47, May 1969.
- ¹⁷Wright R.H., Barger R.L. "Wind tunnel lift interference on sweptback wings in rectangular test sections with slotted top and bottom walls", NASA TR-241, June 1966.
- ¹⁸Berndt S.B. "Inviscid theory of wall interference in slotted test section", AIAA J., Vol. 15, Sept. 1977, pp. 1278-1287.
- ¹⁹Sedin Y.C.-J., Sorensen H. "Computed and measured wall interference in a slotted transonic test section", AIAA Paper 84-0243, Jun. 1984, 14pp.
- ²⁰Glazkov S.A., Gorbushin A.R., Ivanov A.I., Semenov A.V. Recent experience in improving the accuracy of wall interference corrections in TsAGI T-128 wind tunnel., Progress in Aerospace Sciences, Pergamon Press, vol. 37 (2001).
- ²¹Bosniakov S.M., Jitenev V., Fonov S., Shenkin A., Vlasenko V.V., Yatskevich N.S. Method for noise suppressing nozzle calculation and first results of its implementation. "Propulsion and Power", Vol.14, No.1, 1998, pp.101-109.
- ²²MacManus D.G., Eaton J.A. Measurement and analysis of the flowfields induced by suction perforations, AIAA Journal, Vol. 36, No. 9, Sep. 1998, pp. 1553-1561.